JBC RESEARCH ARTICLE

Hydrophobic mismatch is a key factor in protein transport across lipid bilayer membranes *via* the Tat pathway

Received for publication, December 16, 2021, and in revised form, April 13, 2022 Published, Papers in Press, April 28, 2022,
https://doi.org/10.1016/j.jbc.2022.101991

Binhan Hao, Wenjie Zhou, and Steven M. Theg*

From the Department of Plant Biology, University of California, Davis, California, USA

Edited by Karen Fleming

The twin-arginine translocation (Tat) pathway transports folded proteins across membranes in bacteria, thylakoids, plant mitochondria, and archaea. In most species, the active Tat machinery consists of three independent subunits: TatA, TatB, and TatC. TatA and TatB possess short transmembrane alpha helices (TMHs), both of which are only 15 residues long in *Escherichia coli*. Such short TMHs cause a hydrophobic mismatch between Tat subunits and the membrane bilayer, although the functional significance of this mismatch is unclear. Here, we sought to address the functional importance of the hydrophobic mismatch in the Tat transport mechanism in *E. coli*. We conducted three different assays to evaluate the effect of TMH length mutants on Tat activity and observed that the TMHs of TatA and TatB appear to be evolutionarily tuned to 15 amino acids, with activity dropping off following any modification of this length. Surprisingly, TatA and TatB with as few as 11 residues in their TMHs can still insert into the membrane bilayer, albeit with a decline in membrane integrity. These findings support a model of Tat transport utilizing localized toroidal pores that form when the membrane bilayer is thinned to a critical threshold. In this context, we conclude that the 15-residue length of the TatA and TatB TMHs can be seen as a compromise between the need for some hydrophobic mismatch to allow the membrane to reversibly reach the threshold thinness required for toroidal pore formation and the permanently destabilizing effect of placing even shorter helices into these energy-transducing membranes.

The twin-arginine translocation (Tat) pathway, which is found in prokaryotes, archaebacteria, chloroplast thylakoids, and some mitochondria, is able to transport multiple substrate proteins across the membrane lipid bilayers. In chloroplasts, this pathway is responsible for the transport of a number of essential proteins, including two of the three subunits of the oxygen-evolving complex (1). In bacteria, the Tat pathway serves several critical biological processes, including electron transport, cell division, cell wall formation, stress tolerance, and pathogenesis (2, 3). The Tat pathway has the following unusual characteristics. First, it has the ability to transport folded proteins, which is fundamentally different from, for instance, the mitochondrial import and the ubiquitous Sec pathways. Second, Tat pathway substrates have a unique cleavable signal peptide, which carries a nearly invariant pair of arginines (-R-R-) (4). Third, this pathway uses the proton-motive force (PMF) as the sole energy source, with no contribution from NTP hydrolysis (5). Fourth, the Tat pathway acts in an ion-tight manner while transporting substrates of different sizes (6, 7). Fifth, the complete translocation machinery assembles only transiently during the transport event (8). Even though Tat pathway can transport folded proteins with different sizes, the Tat translocon, in most species, involves only three functionally independent subunits, TatA, TatB, and TatC. It has been shown that TatA, TatB, and TatC form a protein complex that serves as the receptor for Tat signal peptide (9–11). The assembly into a functional translocon that includes TatA depends on substrate binding and the PMF. Finally, even though TatB and TatC are present in a 1:1 stoichiometry, TatA joins the complex in variable stoichiometries (12).

The structures of the three Tat subunits have been reported (13–16). TatA and TatB share an overall "L-shape" conformation composed of an N-terminal undefined short region located in the periplasm in bacteria, a remarkably short transmembrane alpha helix (TMH), a hinge region followed by one or more amphipathic helices (APHs), and an unstructured C-terminal tail. In contrast, TatC has six TMHs and is configured in a cupped hand shape with both N-terminal and C-terminal located in the cytoplasm.

Three models have been proposed for the mechanism of protein transport on the Tat pathway. In the first model, TatA is proposed to form a form-fitting proteinaceous pore around the incoming transport substrate (17, 18). In a second model, TatA is thought to act as a coenzyme that accumulates to activate a translocon built from a complex consisting of TatB and TatC (19, 20). A third model posits that under the influence of all Tat subunits, the substrate itself, and the proton-motive driving force, the membrane thins locally until the bilayer breaks down with the formation of lipid-lined toroidal pores through which substrates traverse the membrane (6, 21, 22). Unlike proteinaceous pores in which APHs form water-filled channels (23, 24), in toroidal pores, the lipid molecules wrap across the membrane bilayer to form channels toroidal in shape. A similar lipid toroidal pore model is thought to govern the translocation of antimicrobial peptides across biological membranes (25–27). It has been shown that toroidal pores are

* For correspondence: Steven M. Theg, smtheg@ucdavis.edu.

quite general since they can be induced not only by peptides (28) but also by other chemicals (29). The first and third models are minimally depicted in Figure 1; more detailed representations of toroidal pores and their role in membrane transport can be found (6, 26, 30).

Although there is no detailed information about the structure of the active Tat machinery, a special structural feature in the TatA and TatB TMHs potentially point to an active role of the membrane biophysics in the mechanism of Tat pathway. In *Escherichia coli*, the TMHs of TatA and TatB only have 15 amino acids, respectively, which makes the length of TMHs (~22.5 Å) much shorter than the normal thickness of the hydrophobic core of the membrane (30 Å) (31). The difference between the length of the TMHs and the thickness of membrane bilayer causes a hydrophobic mismatch effect. Many studies have shown that the activity of membrane proteins can be sensitive to such mismatch (32–34). The possible consequences of the hydrophobic mismatch between short TMHs and lipid bilayers are various and depend on the overall topology of the proteins. One of the outcomes is protein aggregation or oligomerization (35), which can cause proximal thinning of the membrane bilayer. Such protein oligomerization phenomenon is also observed in TatA, which forms higher order structures in the resting state of Tat transport (36, 37). It remains unclear that whether such hydrophobic mismatch between Tat subunits and membrane bilayer is necessary for the Tat pathway. A previous study showed that the TMH of TatA (without the APH) can destabilize the membrane in inverted membrane vesicles (IMVs), even though the full-length TatA does not show a similar proton leakage effect. Such membrane destabilization could potentially be involved in the formation of transport-competent toroidal pores (22).

In the present study, we investigate the hydrophobic mismatch between Tat subunits and the membrane bilayer by modifying the length of the TMHs of *E. coli* TatA and TatB. Up to five amino acids were added to the TMHs at three different loci to decrease the hydrophobic mismatch. Conversely, up to four amino acids were deleted from the TMHs to increase the hydrophobic mismatch. The effects of these changes in TMH lengths were examined by three different measures of Tat activity, both qualitative and quantitative. We found that the hydrophobic mismatch between Tat subunits and membrane bilayer appears to be optimized for maximal Tat activity. We further found that decreasing the length of the TatA TMH caused leakage of protons, and presumably other ions, across the membrane. These findings offer the insights into functional importance of the unusually short TMHs of TatA and TatB for the mechanism of Tat translocation.

Results

A conserved 12 amino acid-long hydrophobic region is present in TatA and TatB across different species

The *E. coli* TatA and TatB TMHs each consist of 15 residues (Ile6–Phe20 in the TatA and Phe6–Leu20 in the TatB) according to the NMR structures (16, 38). In *Bacillus subtilis*, a gram-positive bacteria, the $TatA_d$ also includes a TMH with 15 residues (Ile7–Phe21) (13). To assess whether the length of these short TMHs is conserved across different species, 122 TatA and 60 TatB sequences from bacteria, chloroplasts, and mitochondria were aligned by MUSCLE (Fig. 2, *A* and *B*). Consistent with the previous literature (39), Phe(F)-Gly(G) and Gly(G)-Pro(P) motifs were observed in the TatA and TatB alignments, respectively, and a conserved polar amino acid locus (#8 in the TatA and TatB sequence logo plots) was also observed. However, the precise TMH length of TatA/B sequences could not be determined because of lack of structural information for each Tat protein. Furthermore, since there are conserved hydrophilic amino acids present at eighth position in TatA/B (*E. coli* TatA/B numbering, Fig. 2, *A* and *B*), it is also difficult to estimate the TMH length. Even though it is hard to predict accurate length for each TatA/B sequence, a 12-residue hydrophobic region between the polar residue (position #8) and the glycine (position #21) is found to be extremely conserved among all TatA and TatB sequences analyzed. Such conservation of the length of the TatA and TatB TMHs across species, which display somewhat different membrane bilayer thicknesses (31, 40, 41), suggests that the length of the TatA and TatB TMH has potential significance for the Tat transport mechanism.

TMHs with only 15 residues are not common

The 15-residue length of the TatA and TatB TMHs is remarkable in that they are expected to be longer (42) to span

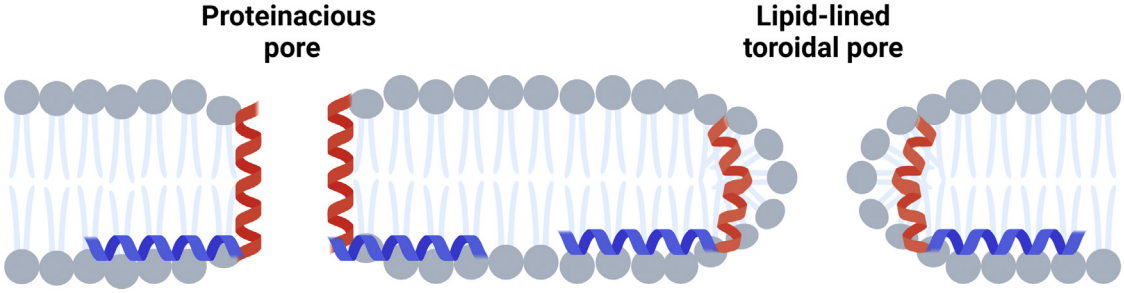

Figure 1. Two models of Tat protein transport. The L-shaped peptide represents the TatA TMH (*red*) and APH (*blue*); the TatA C-terminus is not drawn for simplicity. *Left*, a proteinaceous pore delineated by the TatA TMH (model 1 in text); *right*, a toroidal pore with TatA TMHs buried under the lipid head groups (model 3 in text). APH, amphipathic helix; TMH, transmembrane alpha helix.

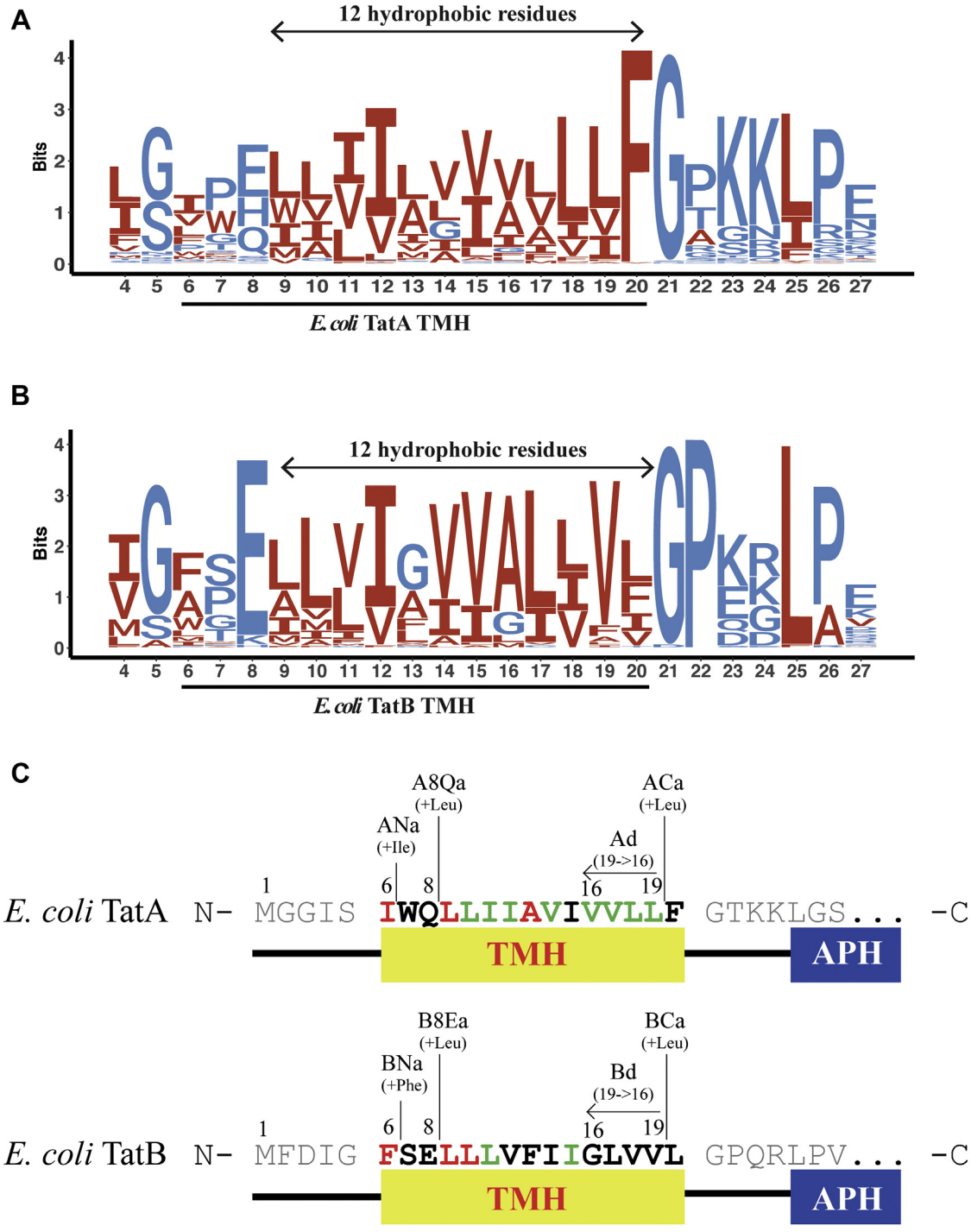

Figure 2. Sequence alignments of TatA and TatB TMH and schematic diagrams for mutant design. *A* and *B*, sequence logos for prokaryotic TatA and TatB alignments, respectively. About 122 TatA sequences and 60 TatB sequences were downloaded from GenBank and subjected to multiple sequence alignment using MUSCLE. Sequence logos were subsequently generated using ggseqlogo in RStudio, where *E. coli* TatA and TatB numbering was used to denote residue locations. Hydrophobic residues were represented in *red*, and hydrophilic residues were represented in *blue*. An invariant 12-residue long hydrophobic region is present in both TatA and TatB and highlighted by *arrows*. *C*, schematic diagram for the design and naming of *E. coli* TatA and TatB TMH mutants. In prose, the first letter in the mutant name, A or B, refers to TatA or TatB, respectively. The next letters and numbers refer to the position of the change; N means at the TMH N-terminus, 8Q or 8E means after the polar amino acid at position 8, C means at the TMH C-terminus; a or d means addition or deletion, respectively, with all deletions occurring at the TMH C-termini. The final number refers the number of amino acids added or deleted at the specified position. Thus, ANa3 is the mutant construct wherein 3 amino acids were added at the N-terminus of the TatA TMH, A8Q2 is the construct wherein 2 amino acids were added after Q8 in TatA, and Bd2 refers to the construct wherein 2 amino acids were deleted from the C-terminus of the TatB TMH. The exact sequences of the different TMH mutants are shown below in Table 1. TMH, transmembrane alpha helix.

the 30 Å hydrophobic core of a typical membrane (Fig. 3*A*). In order to understand how common such short TMH lengths are, we analyzed the TMH lengths in thousands of single-pass proteins from bacteria and chloroplasts. Figure 3*B* demonstrates that, as expected, such short-length TMHs are relatively rare, suggesting again that there is some functional significance to this feature of TatA and TatB.

Experimental modification and nomenclature for TMH-length modifications in TatA and TatB

To better understand how subunit hydrophobic mismatch contributes to Tat transport, we modified the lengths of the TMHs by adding or deleting amino acids from *E. coli* TatA and TatB. Four structural and functional principles were considered to minimize the effect on the overall topology of the TatA and TatB subunits when lengthening or shortening the TMHs. First, as the TMHs are α-helices, modifying the number of amino acids contained therein changes not only the length but also the potential protein-interacting helix faces. In order to minimize the relative rotation from subunit interfaces and APH orientation, amino acids were added close to the helix termini, rather than in the middle. Second, for the same reason, amino acid deletions were performed at the helix C terminus. Third, we avoided deleting the conserved residues and functional groups in the TMHs. Fourth, we added the same amino acids as the one adjacent to the addition location. Based on those principles, three different loci were selected for the addition of one to five amino acids to lengthen the TMHs, and one location was selected to delete one to four amino acids to shorten the TMHs (Fig. 2*C*). The various length mutants include the following: First, the TatA N-terminus addition (ANa) group and the TatB N-terminus addition (BNa) group in which amino acids were added at the extreme N-terminus of

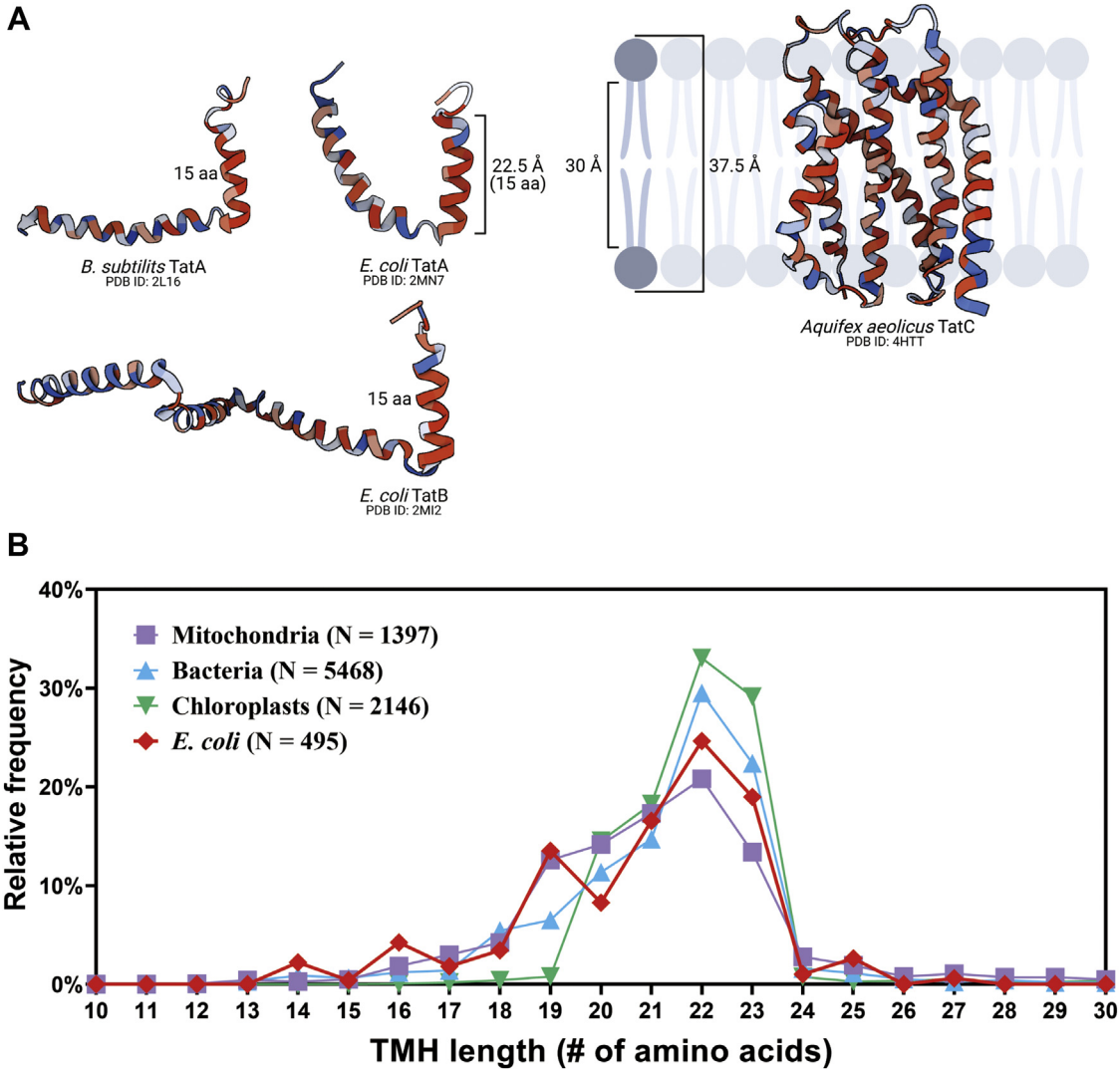

Figure 3. Frequency of short TMHs in selected organelles and organisms. *A*, representation of the hydrophobic mismatch between Tat subunits and the membrane bilayer. Protein structure was obtained from the Protein Data Bank. *B*, statistical analysis of the TMH length of proteins across different species. TMH length for each protein was predicted by TMHMM Server, version 2.0, which was then rounded to the nearest integer. Relative frequency in percentages was obtained by calculating the ratio of the number of proteins with predicted TMH at the indicated length to the total number of proteins in the corresponding category (mitochondria, bacteria, chloroplast, and *E. coli*). N, the total number of entries in each category. Further details are provided in the Experimental procedures section. TMH, transmembrane alpha helix.

the TMHs. Second, the TatA 8th Glutamine addition (A8Qa) group and the TatB 8th Glutamate addition (B8Ea) group in which residues were added immediately following the polar amino acid in the TatA or TatB TMHs. Third, the TatA C-terminus addition (ACa) group and the TatB C-terminus addition (BCa) group, in which residues were added at the extreme C-terminus of the TMHs before the conserved 19th Phe in TatA or the 19th Leu, in the TatB. For deletion mutants, up to four amino acids before the 19th Phe (in TatA) or the 19th Leu (in TatB) were deleted step by step from the C to N-terminus direction and are named the TatA deletion (Ad) group and TatB deletion (Bd) group. For example, "Ad2" represents the mutant whose 19th valine and 18th valine from the TatA TMH were deleted. In this study, we used the low copy pTat101 (43) as the parental plasmid, which constitutively expresses TatA, TatB, and TatC. This plasmid was chosen to express Tat subunits at native expression levels and avoid the potential phenotype variation because of overexpression of Tat subunits. Table 1 shows the detailed design described previously for all the mutants.

TatA and TatB deletion mutants exhibited lower membrane insertion stability

An obvious challenge for membrane proteins with short TMHs is correct and stable insertion into the membrane. To assess the membrane stability of our mutant proteins, membranes were isolated from whole cells and treated with 100 mM sodium carbonate to wash off nonintegrated membrane proteins (44). According to the Western blot results (Fig. S1), all the TatA and TatB addition mutants exhibited the expected stable membrane insertion ability. In contrast, a decrease in the membrane abundance was observed in the Ad and Bd deletion groups (Fig. 4, *A* and *B*). The amount of membrane-embedded TatA in the Ad group averaged approximately 20% of the amount found in the wt (Fig. 4*A*). Similarly, all Bd mutants displayed less abundance compared with the wtTatB (Fig. 4*B*). It is surprising that the Ad4 TatA and Bd4 TatB, which have only 11 amino acids in the TMH, were still detected in the membrane fraction. Previous research (45) showed that TatB and TatC tend to form a TatBC complex in a one-to-one stoichiometry in the resting state of the Tat translocon. To test whether the TatC contributes to the membrane stability of the TatB deletion group, TatC was knocked out in the Bd4 mutant (*i.e.*, Bd4*ΔtatC*). Even though a significant amount of Bd4 TatB was present in the membrane fraction when TatC was present, no Bd4 TatB was detected in the membrane of the Bd4*ΔtatC* mutant (Fig. 4*C*). This is clear evidence that TatC stabilizes TatB in the membrane such that TatB can be embedded when its TMH is too short to remain in the membrane on its own.

In summary, lengthening the TMHs of TatA and TatB did not significantly affect their membrane stability. Oppositely, even though Ad4 TatA and Bd4 TatB could still insert into the membrane, shortening the TMHs diminished the membrane stability of both TatA and TatB mutants. In addition, TatC, by forming a protein complex with TatB, appears to assist the TatB mutants possessing shorter TMHs to stably embedded in the membrane.

E. coli *TatA activity is diminished by lengthening or shortening the TatA TMH*

As a first pass at assessing the Tat activity of TatA TMH length mutants, we examined their growth profiles in SDS-containing media. Two native *E. coli* Tat substrates, AmiA and AmiC, facilitate cell wall modeling, and a defect in transporting those substrates results in sensitivity of the cell envelope to SDS in the media (2). Accordingly, growth in SDS-containing media is a convenient indicator of whether cells

Table 1
Summary of growth performance in the presence of SDS for TatA and TatB mutants

Name	TatA TMH sequence	Length (residues)	Growth in SDS	Name	TatB TMH sequence	Length (residues)	Growth in SDS
wtTatA	IWQLLIIAVIVVLLF	15	+++	wtTatB	FSELLLVFIIGLVVL	15	+++
ANa1	**I**IWQLLIIAVIVVLLF	16	+++	BNa1	F**F**SELLLVFIIGLVVL	16	+++
ANa2	**II**WQLLIIAVIVVLLF	17	—	BNa2	F**FF**SELLLVFIIGLVVL	17	+++
ANa3	**III**WQLLIIAVIVVLLF	18	—	BNa3	F**FFF**SELLLVFIIGLVVL	18	+++
ANa4	**IIII**WQLLIIAVIVVLLF	19	—	BNA4	F**FFFF**SELLLVFIIGLVVL	19	+++
ANa5	**IIIII**WQLLIIAVIVVLLF	20	—	BNa5	F**FFFF**FSELLLVFIIGLVVL	20	+
A8Q1	IWQ**L**LLIIAVIVVLLF	16	+++	B8Ea1	FSE**L**LLLVFIIGLVVL	16	—
A8Q2	IWQ**LL**LLIIAVIVVLLF	17	+++	B8Ea2	FSE**LL**LLLVFIIGLVVL	17	—
A8Q3	IWQ**LLL**LLIIAVIVVLLF	18	+++	B8Ea3	FSE**LLL**LLLVFIIGLVVL	18	—
A8Q4	IWQ**LLLL**LLIIAVIVVLLF	19	+++	B8Ea4	FSE**LLLL**LLLVFIIGLVVL	19	—
A8Q5	IWQ**LLLLL**LLIIAVIVVLLF	20	—	B8Ea5	FSE**LLLLL**LLLVFIIGLVVL	20	—
ACa1	IWQLLIIAVIVVLL**F**	16	+++	BCa1	FSELLLVFIIGLVV**L**L	16	—
ACa2	IWQLLIIAVIVVLL**LF**	17	+++	BCa2	FSELLLVFIIGLVV**LL**	17	—
ACa3	IWQLLIIAVIVVLL**LLF**	18	++	BCa3	FSELLLVFIIGLVV**LLL**	18	—
ACa4	IWQLLIIAVIVVLL**LLLF**	19	+++	BCa4	FSELLLVFIIGLVV**LLLL**	19	—
ACa5	IWQLLIIAVIVVLL**LLLLF**	20	—	BCa5	FSELLLVFIIGLVV**LLLLL**	20	—
Ad1	IWQLLIIAVIVVL-F	14	+++	Bd2	FSELLLVFIIGLV-L	14	+
Ad2	IWQLLIIAVIVV–F	13	++	Bd2	FSELLLVFIIGL–L	13	++
Ad3	IWQLLIIAVIV—F	12	++	Bd3	FSELLLVFIIG—L	12	—
Ad4	IWQLLIIAVI——F	11	—	Bd4	FSELLLVFII——L	11	+++

Growth performance is described by the following symbols. +++, cells exhibited higher than 50% survival percentage in 10% SDS; ++, cells exhibited higher than 50% survival percentage in 5% SDS; +, cells exhibited higher than 10% survival percentage in 5% SDS; –, cells exhibited less than 10% survival percentage in 5% SDS. Survival ratios were calculated as absorbance at 600 nm of cells grown for 5 h in the presence of SDS to those grown in the absence of SDS. Detailed survival rates in media with different concentrations of SDS are shown in Fig. S2. The sequences show the positions and amino acids added (*bold letters*) or deleted (*bold* —) for the various mutants

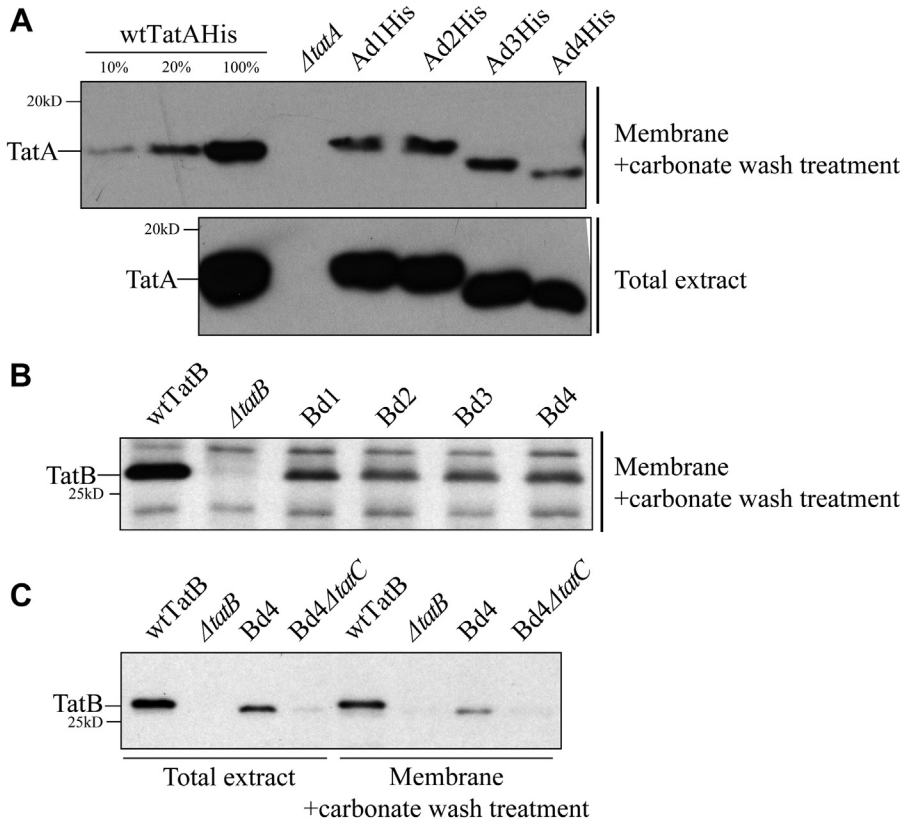

Figure 4. Shortening the TatA and TatB TMH lengths results in lowered membrane stability. *A*, assessment of membrane stability in TatA deletion mutants. Total cell extract of C-terminal 6× His-tagged wtTatA (wtTatA-His), *ΔtatA*, and TatA deletion mutants (Ad1-4His) was subjected to fractionation. Membrane fractions (*upper gel*) were recovered from total cell extracts (*lower gel*) and washed with 100 mM Na_2CO_3 to remove the portion of TatA, which failed to stably embed in the membrane. Immunoblots using anti-His antibody are shown. Lanes 1 to 3, serial dilution of membrane-embedded TatA in wt cells. *B*, $NaCO_3$-washed membrane fractions isolated from cell extracts of wtTatB, *ΔtatB*, and TatB deletion mutants (Bd1–4). Immunoblot using anti-TatB antibody is shown. *C*, Na_2CO_3-washed membrane fractions (*right*) isolated from cell extracts (*left*) of wtTatB, *ΔtatB*, Bd4, and Bd4 in a TatC knockout strain (Bd4*ΔtatC*). Immunoblot using anti-TatB antibody is shown. TMH, transmembrane alpha helix.

have at least a minimal Tat transport capability. Table 1 summarizes the survival ratio after 5 h growth on SDS-containing LB media for our TMH length mutants; individual survival ratio curves are shown in Fig. S2. A number of notable points are seen in this table.

First, of all the members of the ANa group, only ANa1 could grow in LB medium with 5% SDS and the rest lost their ability to grow with as low as 1% SDS (Fig. S2). In contrast, both A8Qa1–4 and ACa1–4 mutant groups were able to grow in LB medium with 5% SDS, whereas neither A8Qa5 nor ACa5 could survive in the same media. For the TatA deletion group, surprisingly, all the Ad mutants except the Ad4 could grow in LB medium with 5% SDS. Specifically, the Ad3 mutant, whose TMH only contains 12 amino acids, still retained the ability to grow in LB medium with 5% SDS.

While the SDS-growth assay is convenient, it is not obvious how it scales with absolute Tat activity. To examine our mutants more quantitatively, we monitored the transport of a native Tat substrate, SufI, to the periplasm 2.5 h after induction with IPTG in the presence of TatA mutants in a TatBC background. This assay, while still essentially an end-point assay, has the potential to provide a more fine-grained view of Tat activity than the SDS-growth assay. The results of this *in vivo* transport assay, shown in Figure 5 as representative gels from two experiments, display many of the features observed in the SDS-growth assay. For instance, ACa1, ACa2, and ACa4 mediated SufI transport (Fig. 5*B*) in addition to growth on SDS, as is the case also with the deletion mutants Ad1, Ad2, and Ad3 (Fig. 5*C*). Neither ACa5 nor Ad4 showed SDS growth or SufI *in vivo* transport (Fig. 5, *B* and *C*). However, it is clear that none of the mutants that could grow on SDS transported SufI as efficiently as did the wtTatA. As an example, see the A8Qa mutants in Figure 5*A* or any of the mutants in Figure 5, *B* and *C*. Thus, the *in vivo* SufI transport assay leads to the conclusion that either lengthening or shortening the TatA TMH results in loss of Tat transport efficiency, suggesting that there is a functional reason for its 15 amino acid length.

An even more fine-grained assessment of Tat transport activity is offered in pulse-chase assays. Here, kinetics of transport can quantitatively indicate the true extent to which the TMH length mutants operate compared with the wt. As seen in Figure 6, *B* and *D*, whilst the wtTatA transported SufI with initial velocity (V_0) of 77.1×10^{-3} min^{-1}, the next best C-terminal addition mutant, ACa1, operated with a rate constant only 19% of that value. The best performing deletion mutant, Ad2, operated with a rate constant 48% of the wt (Fig. 6, *C* and *D*). Here, when a true quantitative comparison of the TatA TMH length mutants is undertaken, it can again be concluded

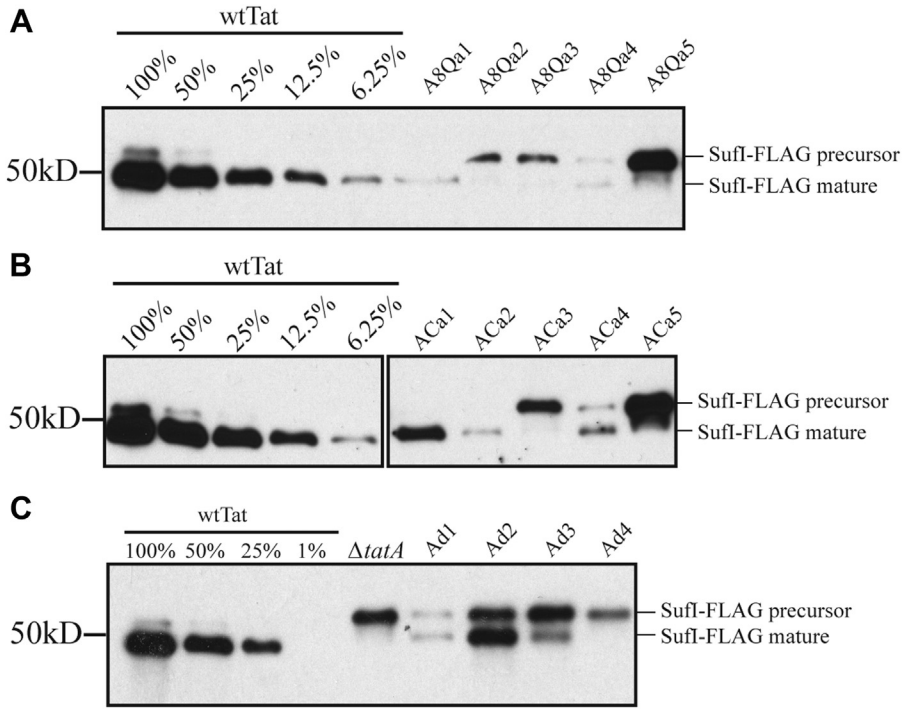

Figure 5. *In vivo* transport of SufI in TatA TMH length mutants. Periplasmic fractions were prepared from wtTat, TatA knockout mutant (*ΔtatA*), and TatA mutant cells transporting FLAG-tagged SufI (SufI-FLAG) 2.5 h after induction with 1 mM IPTG. The number of cells used in periplasmic extraction was normalized based on absorbance at 600 nm, and immunoblots were developed using anti-FLAG antibody. Precursor and mature forms of SufI-FLAG are labeled. *A*, transport of SufI-FLAG in the AQ8a group (AQ8a1–5). *B*, transport of SufI in the TatA C-terminal addition group (ACa1–5). *C*, transport of SufI-FLAG in the TatA deletion group (Ad1–4). TMH, transmembrane alpha helix.

that the 15-residue wt length appears to be tuned for optimal activity.

Overexpression of Ad3 and Ad4 blocks Tat transport

The majority of TatA is known to be recruited to the TatBC complex after the complex binds to the precursor signal peptide (8, 36, 46, 47). Since the optimal number of TatA is reported to be ∼20-fold higher than the TatB and TatC in the translocon (12, 48), insufficient TatA in the membrane is a possible reason for lowering of the overall transport rate when the TMH is shortened below 15 amino acids.

To determine if the lower abundance of the TatA in the Ad mutants caused the decrease in the Tat activity, wtTatA and the Ad1–Ad4 TatA mutants were overexpressed on a separate plasmid, which was induced by arabinose. Both wtTatA, and the first three deletion mutants, Ad1, Ad2 and Ad3, and less so for Ad4, accumulated to higher levels after overexpression (Fig. 7*A*). This resulted in transport of a slightly higher amount of SufI-FLAG to the periplasm in the wt and the first two TatA deletion mutants, Ad1 and Ad2 (Fig. 7*A*). In contrast, SufI-FLAG was not transported when the shortened TatA mutants Ad3 and Ad4 were induced by arabinose, even though they accumulated to levels exceeding or just below that of wtTatA, respectively. When a gradual increase of arabinose concentration was applied to induce increasing amounts of Ad3 TatA, the amount of mature SufI-FLAG was decreased in a dose-dependent manner, indicating that overexpressed Ad3 TatA blocked Tat transport (Fig. 7*B*). Furthermore, when Ad3 and Ad4 TatA mutants were overexpressed in wtTat background, they inhibited SufI-FLAG transport even in the presence of fully functional wtTatA (Fig. 7*C*). These experiments demonstrate that while overexpressing Ad1 and Ad2 TatA could slightly improve the Tat transport activity, overexpressing Ad3 and Ad4 TatA exhibited a dominant negative-like effect. They also show that the relative low abundance of Ad3 and Ad4 TatA in the membrane is not the reason for the low Tat activity seen in Figures 5 and 6.

A similar dominant negative effect was seen when the ACa mutants were overexpressed in the presence of wtTatA (Fig. 7*D*). It can be seen that none of ACa group mutants exhibited high transport activity when overexpressed with 0.2% arabinose. The ACa2–5 mutants especially displayed significantly lower transport when overexpressed with wtTat, even though their effects were not as severe as with the Ad3 and Ad4 mutants (Fig. 7*C*). These experiments show that overexpression of both the Ad and ACa group mutants did not lead to improved Tat transport activity but rather blocked transport in the more severe cases.

TatA mutants with shortened TMHs compromise membrane integrity

It has been previously demonstrated that the TatA TMH (without the APH) can compromise membrane integrity in IMVs (22). In our study, we asked whether a similar effect would be seen with our TatA mutants, which have shortened TMH. wtTatA, Ad TatA, or ACa TatA was overexpressed with either constitutively expressed TatBC or in the DADE-A strain (*Δtat*) background. Relative membrane abundance was also

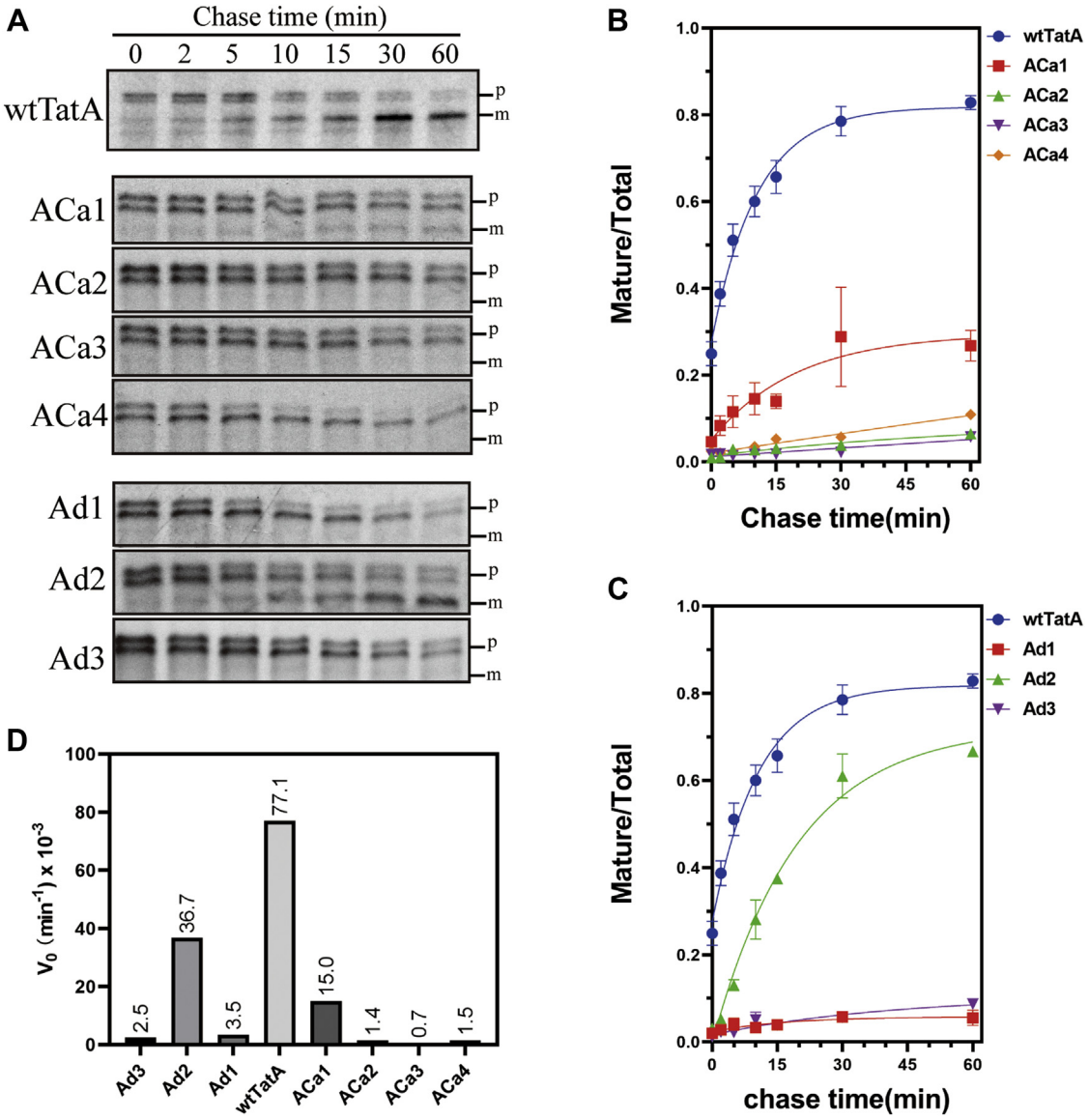

Figure 6. Pulse-chase assays with TatA TMH length mutants. *A*, SufI transport activity supported by TatA addition and deletion mutants (ACa1–4 and Ad1–3), as monitored by pulse-chase experiments. Autoradiograms developed from 8 to 16% acrylamide gels are shown; gels are representative of at least two biological replicates. *B* and *C*, quantitation of the gels in *A*. The ordinate represents the ratio of intensities of the mature bands divided by the intensities of the mature + precursor bands. Data were fitted to a rising exponential model, and the corresponding initial velocity (V_0) is shown in (*D*). m, mature SufI; p, precursor; TMH, transmembrane alpha helix.

tested by immunoblot (Fig. S3). Acridine orange was used to detect the ΔpH across the IMV membrane (Fig. 8). Lower ΔpH was interpreted as an increased proton leak.

In these experiments, we found first, that wtTatA actually assisted in maintaining membrane integrity, which is counterintuitive since TatA possesses a short TMH. Second, Figure 8*A* shows that the membranes developed a progressively lower pH gradient (less quenching of the fluorescence signal after adding ATP) when the TMH of TatA was progressively shortened. This result was not related to relative TatA abundance (Fig. S3). In addition, Ad4 TatA, which showed no Tat activity, caused the highest membrane leakage compared with TatABC or TatBC IMVs. Third, no such effect was observed in TMH-lengthened ACa group mutants, with the exception that ACa5BC IMVs displayed similar membrane leakage as TatBC IMVs (Fig. 8*C*). These effects were manifested in the absence (Fig. 8, *B* and *D*) of TatBC as well. The Ad4 TatA mutant displayed a similar membrane leakage effect as the no Tat strain. In contrast, the ACa mutants, which possess longer TMHs than wtTatA, displayed much lower membrane leakage than the wtTatA (Fig. 8*D*). We conclude from these experiments that, longer TatA proteins can assist in maintaining membrane integrity in the IMVs, whereas shorter TatA TMHs resulted in a loss of membrane integrity. The Ad4 TatA in the presence of TatBC caused the highest membrane leakage among all the mutants tested. Such result suggests a general increase in membrane instability when shortening the TMH, which explains why the shorter TMH TatA mutants exhibited lower transport rates than wtTatA in spite of their increased hydrophobic mismatch.

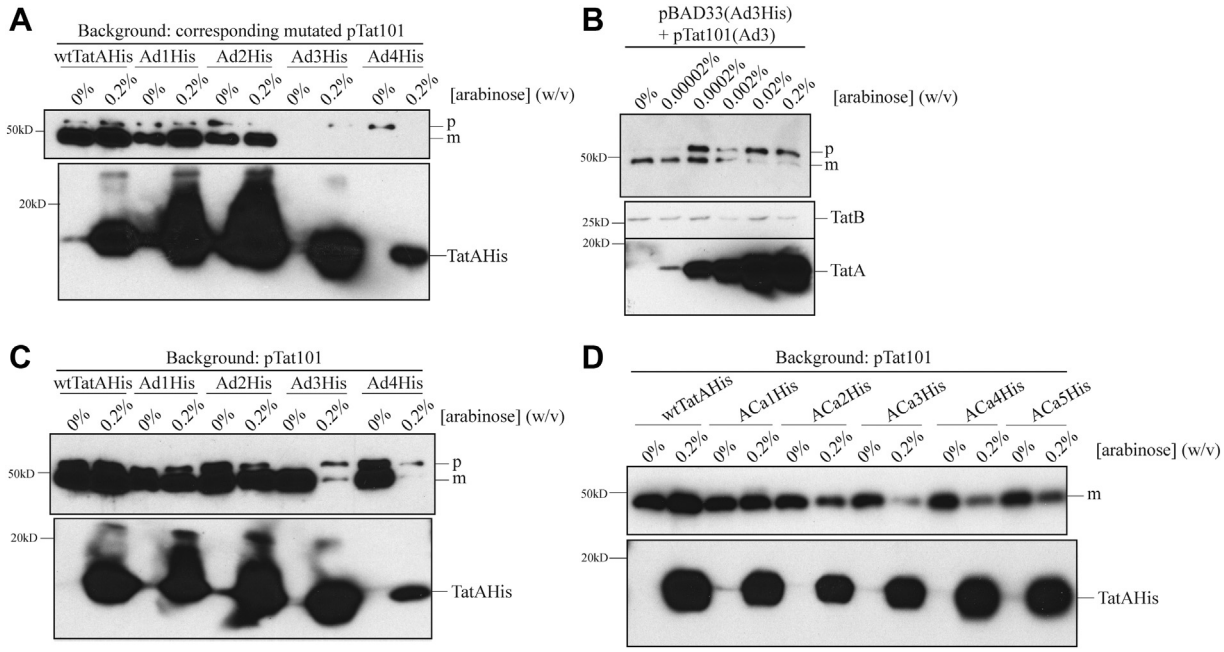

Figure 7. Effect of overexpression of TMH-shortened TatA on SufI transport. *A, in vivo* transport of SufI utilizing indicated mutants. Indicated cells were grown in the presence of indicated [arabinose] for overexpression (from pBAD33) and with the same mutant constitutively expressed as per prior experiments (from pTat101). When the cells reached absorbance of 0.7 at 600 nm, preSufI-FLAG was induced by addition of 1 mM IPTG and then harvested, and periplasm prepared there after an additional 2.5 h. The number of cells used in the periplasm extraction was normalized based on absorbance at 600 nm. An immunoblot using anti-FLAG antibody is shown (*upper gel*). Membrane fractions were isolated, carbonate washed, and samples were then subjected to immunoblotting using the His-tag antibody probing for TatA (*lower gel*). *B*, the experiment of *A* was performed with Ad3 only at the indicated arabinose concentrations, and the immunoblot in the lower gel was in addition probes with anti-TatB as a loading control. *C*, the experiment of *A* was performed with wtTatA expressed as in previous experiments from pTat101 whilst the indicated TatA TMH length mutants were overexpressed from pBAD33 (when arabinose was present). *D*, *in vivo* transport of SufI with overexpressed ACa group TatA under pTat101–DADE-A background. *Upper gel*, periplasm fraction. *Lower gel*, membrane fraction after sodium carbonate wash. Experimental conditions were essentially same as (*C*). m, mature SufI-FLAG; p, precursor; TMH, transmembrane alpha helix.

E. coli *TatB tolerates a wider range of TMH lengths than does TatA*

As previously described, the SDS-growth assay was conducted with the TatB mutants as well. For TatB addition group, the BNa mutants survived in LB medium with 5% SDS, although BNa5 displayed a lower survival ability compared with other BNa mutants (Table 1). Gradual decrease in Tat activity was nonetheless observed in both *in vivo* transport assays (Fig. 9*A*) and pulse-chase experiment (Fig. 10, *A*, *B* and *D*). The BNa1, BNa2, and BNa3 mutants retained approximately 58%, 13%, and 3.5% of the wtTatB V_0, respectively. In contrast, none of B8Ea and BCa group mutants exhibited SDS tolerance, indicating that no Tat transport occurred in those mutants.

In contrast to the TatB addition mutants, a special pattern in the TatB deletion group mutants in terms of SDS tolerance was identified. The Bd1, Bd2, and Bd4 mutants retained sufficient Tat activity to grow in LB medium with 5% SDS, whereas the Bd3 mutant did not. However, pulse-chase experiments with the Bd group indicated that only approximately 5% transport activity was retained in the Bd1, Bd2, and Bd4 mutants (Fig. 10, *C* and *D*). This speaks to the coarseness of the correlation between growth on SDS-containing media and the absolute Tat activity (see Discussion section).

To summarize, these results indicate an acceptable range from 11 to 20 amino acids in the TatB TMH, which is wider than the range proposed from the TatA mutants. As with TatA, a change in the length of the conserved hydrophobic region in the TatB TMH is not favored. Even though an overall longer TMH inhibits the TatB function, if the length of the hydrophobic region is preserved (*i.e.*, adding residue from the N terminus), its negative impact is not as severe when the length of the hydrophobic region is altered.

Discussion

In this study, the effect of the hydrophobic mismatches in the Tat translocon was examined by modifying the length of the TMHs in *E. coli* TatA and TatB. Growth on SDS-containing media, *in vivo* transport and pulse-chase assays were conducted to evaluate the Tat transport activity in the TMH length mutants comprehensively. The results showed that while both TatA and TatB can tolerate some length modification in their respective TMHs, none of the modified mutants transported Tat substrates as well as the wt strain. Interestingly, TatA and TatB exhibited different acceptable lengths of their TMHs, with TatA tolerating a TMH 11 to 19 residues long and TatB tolerating a length between 10 and 20 residues. Further comparison of the transport rates between the addition and deletion mutants revealed different behaviors of the TatA and TatB TMH length mutants, perhaps reflecting their different roles in the Tat transport mechanism.

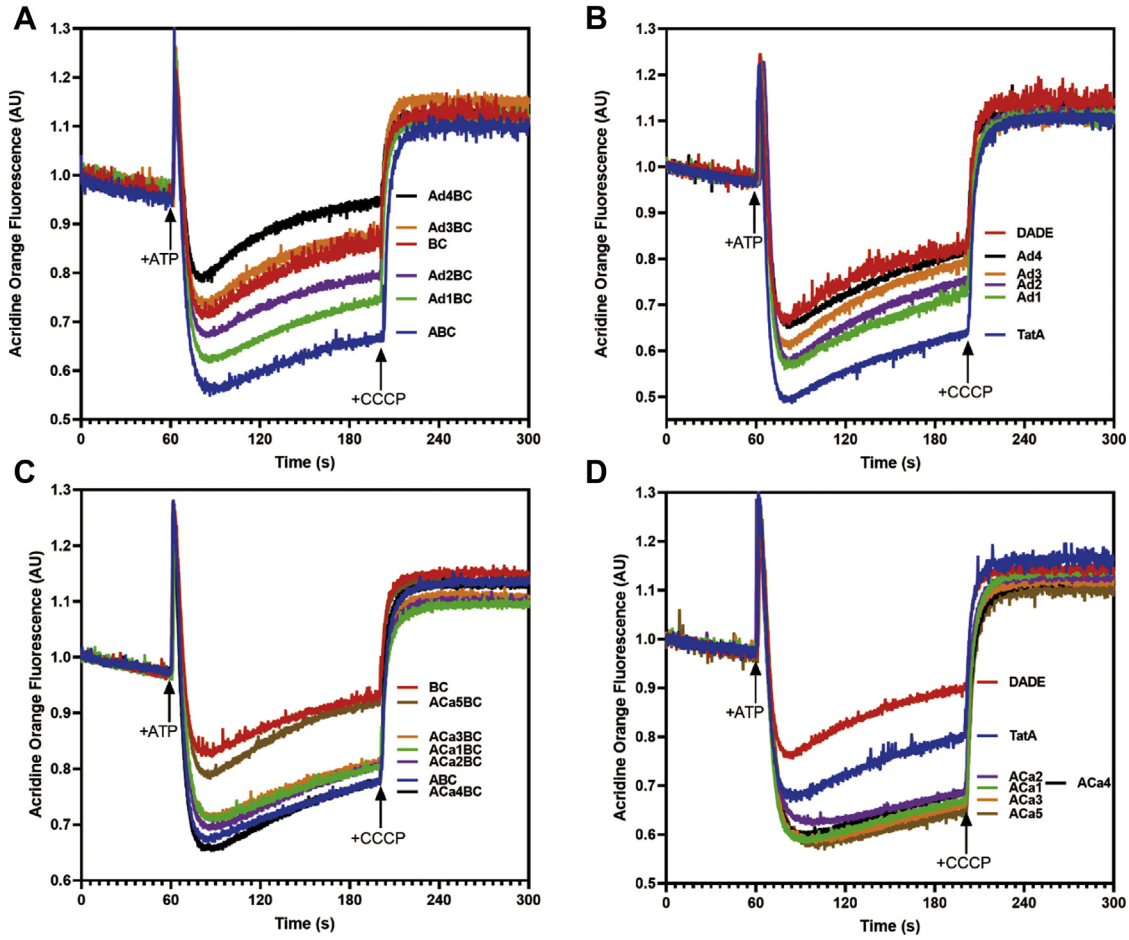

Figure 8. Shortened TatA TMH can cause membrane leakage. The ΔpH developed across IMVs was monitored by quenching of acridine orange. About 4 mM ATP was added at 60 s to generate the ΔpH; 10 μM CCCP was added at 200 s to dissipate the ΔpH, leading to fluorescence recovery. *A* and *C*, ΔpH in TatBC IMVs alone or with the corresponding TatA variants. *B* and *D*, ΔpH in DADE (complete Tat knockout) IMVs alone or with the corresponding TatA variants. AU, arbitrary unit; IMV, inverted membrane vesicle; TMH, transmembrane alpha helix.

It is important to stress that TMHs both lengthened or shortened did not support protein transport as well as the wt 15 amino length TMHs of both TatA and TatB. This, along with the observations that the 15-residue length of these TMHs is conserved (Fig. 2, *A* and *B*), and moreover, this length is relatively rare in single-pass membrane proteins (Fig. 3*B*),

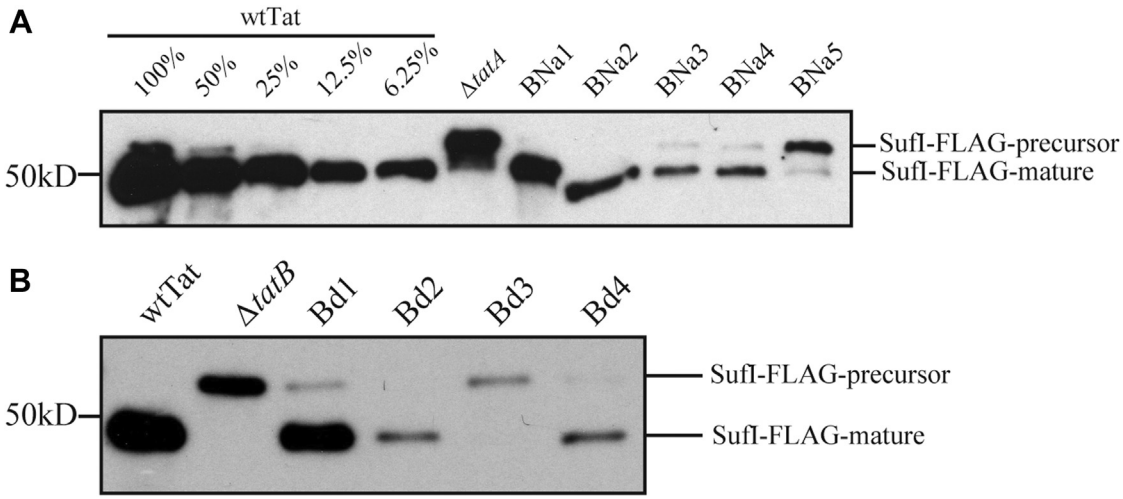

Figure 9. *In vivo* transport assays with TatB mutants. Experiments were performed essentially as for Figure 5 but substituting the TatB TMH length mutants that grew on SDS for the TatA mutants of that figure. *A*, transport of SufI-FLAG in the BNa TatB addition group. *B*, transport of SufI-FLAG in the Bd TatB deletion group. Bd, TatB deletion; BNa, TatB N-terminus addition; TMH, transmembrane alpha helix.

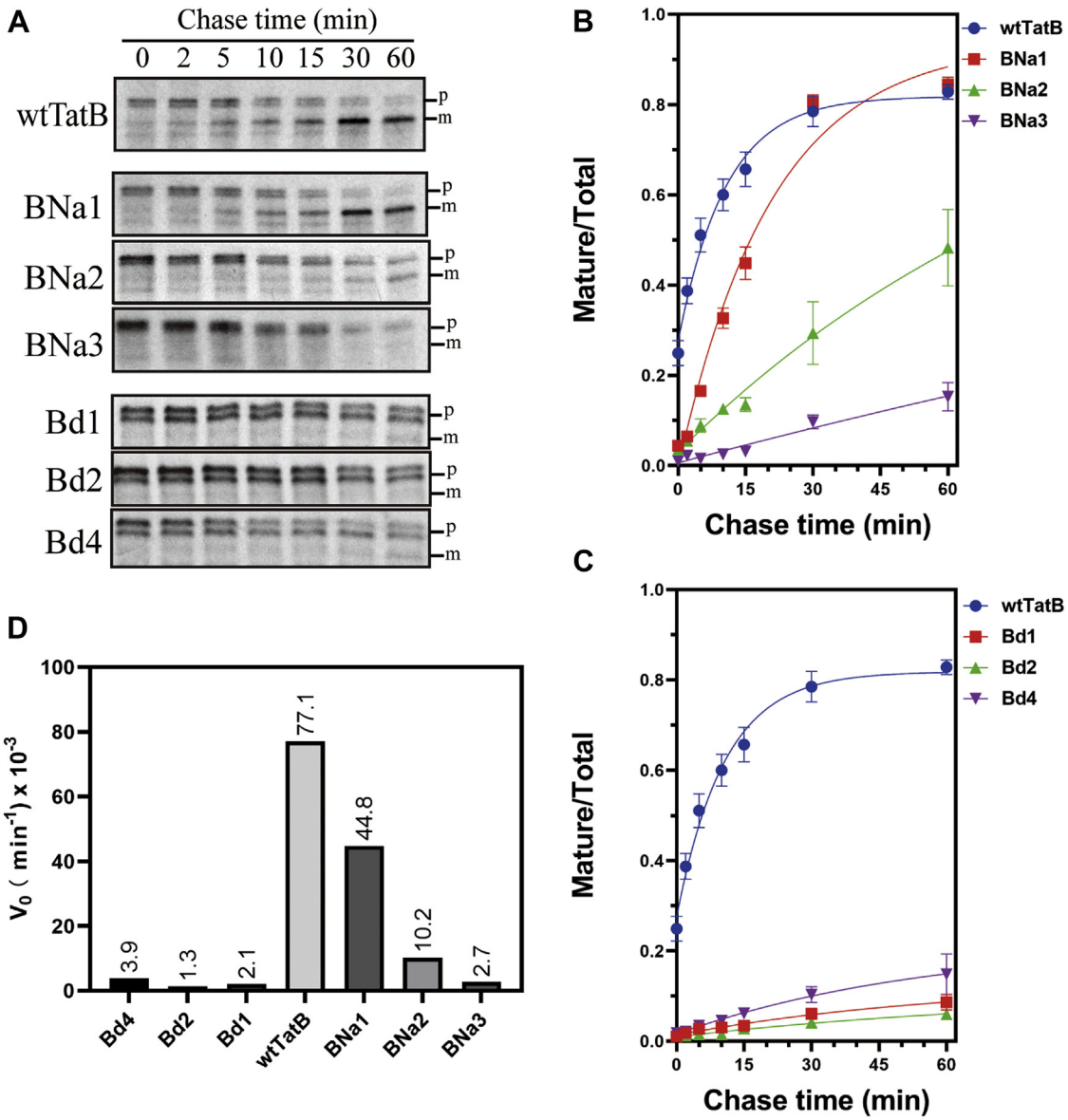

Figure 10. Pulse-chase assays with TatB TMH length mutants. Experiments were performed essentially as for Figure 6 but substituting the TatB TMH length mutants that grew on SDS for the TatA mutants of that figure. *A–D*, SufI transport activity supported by TatB addition and deletion mutants (BNa1–3 and Bd1, 2, and 4), as monitored by pulse-chase experiments. Details are as described for Figure 6. Bd, TatB deletion; BNa, TatB N-terminus addition; TMH, transmembrane alpha helix.

suggests that this particular hydrophobic mismatch is evolutionarily tuned for maximum activity. We are not the first to propose that this plays a role in the mechanism of Tat protein transport (22, 49).

One complicating issue in interpreting the fall off in activity of the TMH length mutants is the fact that amino acids in these TMHs interact with other residues, both in the same polypeptide and in TatC. Coevolution analysis predicted as many as 10 interactions between the TatA TMH residues and those on helices 5 and 6 in TatC (50). Were we to add or delete additional amino acids directly into the middle of the TatA TMH, for instance, then we could expect to disrupt such interactions as positions of amino acids arrayed on the interacting face of the helix would have been altered. To minimize this potential complication, we added residues to the extreme N and C-termini of the TMHs. Addition or deletion of residues form the C-terminus would be expected to keep the presentation face of the TMH intact, while possibly changing its orientation with respect to the APH. This is illustrated in Figure 11, which shows that in the wt proteins, the APHs of both TatA and TatB are displaced approximately 100° to 120° from their respective polar amino acids. The importance of this relative displacement is not obvious, as growth on SDS-containing media cannot be predicted by proximity in the helical wheel projection of the APH to the polar amino acid. Nonetheless, amino acid additions at the extreme C-terminus would be expected to maintain the presenting face of the TMH, and in the case of the ACa mutants, all interacting residues should be intact and in position.

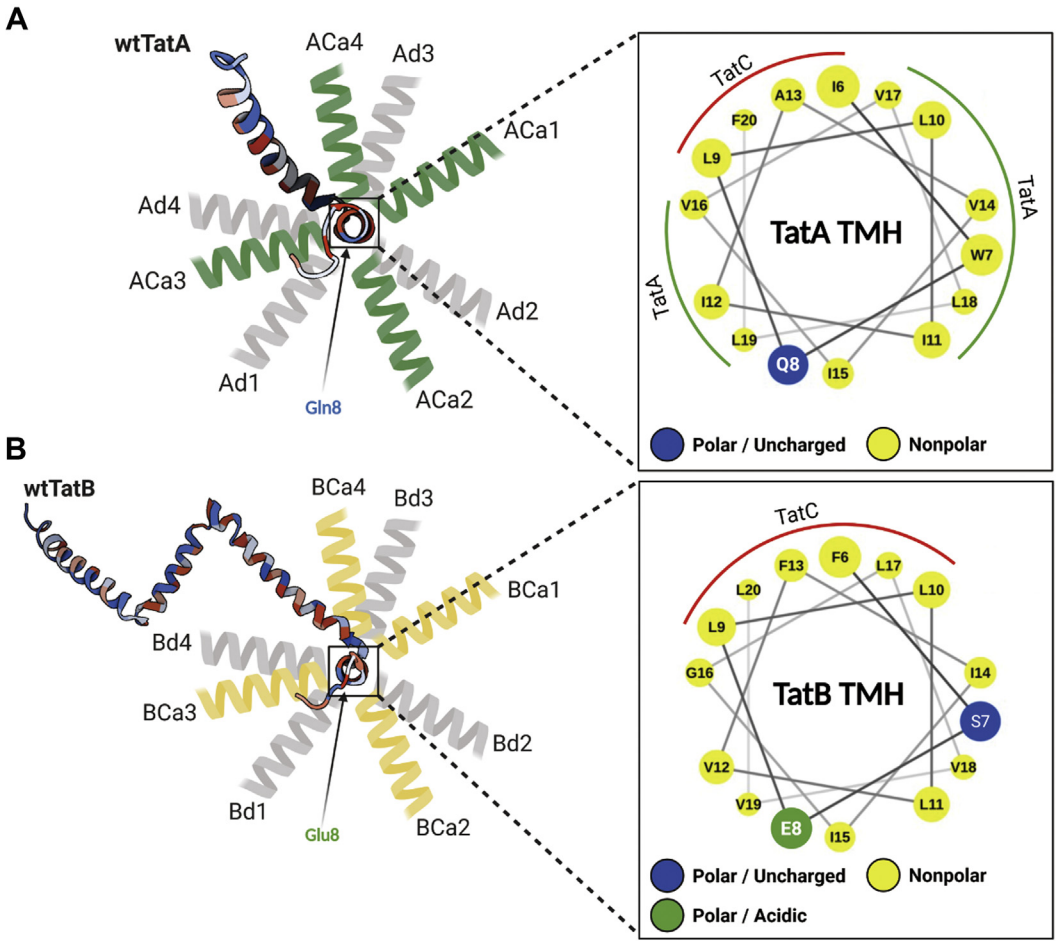

Figure 11. Possible APH orientations change in TatA and TatB TMH mutants. Predicted TatA (*A*) or TatB (*B*) APH orientations are illustrated from the *top view*. The projected structures of wtTatA (Protein Data Bank ID: 2MN7) and wtTatB (Protein Data Bank ID: 2MI2) showing the possible orientation of the APHs with respect to nonvariant polar amino acid positions are shown on the *left*. On the *right* is shown a helical wheel projection (51) showing the potential Tat subunit interaction faces. APH, amphipathic helix; TMH, transmembrane alpha helix.

A less complex situation is expected when amino acids are added to the N terminus of the TMH. In this instance, only the extreme N terminus of the protein should rotate relative to the TMH, with the only potential contact disrupted being the fifth amino acid in either TatA (G5) or TatB (S5); all other residues are intact and in position. Still, one possible effect of such N-terminal addition mutants could be that they push the polar amino acid at position 8, which was shown to be functionally important (52), deeper into the middle of the membrane.

We further considered the possibility that extended-TMH TatA variants do not support protein translocation because they are too long to fit comfortably into the TatBC complex. However, this seems an unlikely explanation because the ACa mutants exhibit a dominant negative effect when overexpressed in the presence of wtTatA. In that experiment, we would not expect the lengthened TatA mutant to displace the wtTatA if it does not fit into the TatA binding site in the first place. Second, it has been reported that TatA and TatB might switch contact positions with TatC in the presence of substrates (10). In this study, we show that TatB can tolerate a larger range of TMH lengths than TatA, especially for the BNa mutants (Fig. 10). If the receptor complex could only fit a TatA or a TatB TMH of a particular size, we might expect identical inhibitory behaviors of the TMH length mutants of these two proteins; we did not. Accordingly, we look to other explanations for their inhibition of protein transport beyond an inability to bind to the TatBC complex.

It is perhaps unexpected that the deletion mutants as short as 11 residues were still able to take up residence in the membranes and resist extraction by carbonate. However, examples of short peptides integrating into both artificial and biological membranes are known from the literature (53–55). In addition, several studies have shown that soluble TatA is able to be functionally incorporated into thylakoid membranes (20, 36, 56–59). The TatB Bd4 mutant loses its membrane location in the absence of TatC (Fig. 4*C*), which points to a stabilizing interaction between the short TatB and TatC. However, the TatA Ad4 mutant appears to embed in the membrane on its own. This is demonstrated not only by their retention in the membranes after carbonate washing but also by the dominant negative-like effect on SufI transport of Ad3 and Ad4 overexpression in the presence of wtTatA and by their ability to cause proton leakage in IMVs.

Our analyses of our TMH length mutants revealed an important technical point about assays for Tat activity. Given that the ANa mutants (except ANa1 mutant) were unable to grow in the presence of SDS, we were surprised that the ACa mutants could indeed grow on the same SDS-containing media. It was only when we performed kinetic assays that it became clear that the Tat activity in the ACa mutants was quite low. Even the best performing TatA C-terminal addition mutant, ACa1, transported SufI at only about 19% of that of the strain harboring wtTatA (Fig. 6*B*). Accordingly, the SDS-growth assay, which is an end-point assay, does not scale linearly with Tat activity and generally indicates only the complete loss of Tat function. Even ACa2, which transports SufI at 1.8% the rate of wt showed wt-like survivability on up to 10% SDS. Assays of Tat function by monitoring the presence of SufI in the periplasm are somewhat more sensitive to absolute Tat activity, but again, this is an end-point assay that may underestimate the negative impact of an altered Tat machinery.

We were surprised to see the different effects of amino acid addition after the polar residues in TatA and TatB. While the amount of SufI found in the periplasm in the TatA A8Qa mutants was generally quite low (Fig. 5*A*), they retained enough activity for growth in the presence of SDS. This contrasted the similar additions in TatB after the E8 residue, which apparently had no remaining Tat activity. This is just one example of many in which lengthening the TMH of TatA produced a different effect than a similar change in the length of the TMH of TatB. It is tempting to attribute this to a proposed fundamentally different function of these two proteins in the mechanism of Tat transport.

We also found that lengthening additions were sensitive to their location relative to the polar amino acids in these TMHs. In both TatA and TatB, additions made at the extreme N terminus of the TMH had different effects than those made just two residues further into the helix, after the polar amino acids. Additions made after the seventh amino acid, but just before the eighth polar residue, had the same growth profile in SDS as the N-terminal additions (Fig. S2). The reason that the addition phenotypes switch around the polar residues remains to be elucidated, but possibilities include disruption of the helix-interacting faces and changes of the depth of the polar amino acids in the membrane.

How do these TMH length mutants inform us about the mechanism of protein transport on the Tat pathway? We knew already that the 15 amino acid length of the TatA and TatB TMHs are evolutionarily optimized by the fact that this length is so conserved. Our experiments now point to why this is the case. It is clear that changing the TMH lengths of either TatA or TatB from 15 residues in either direction results in a decline in overall Tat activity. One could argue that this decline in the TatB TMH mutants might be related to a loss of its ability to interact with TatC correctly, although the advantage conferred by making additions at the N terminus of the TMH are still in effect. Still, since TatB and TatC form a stable complex with a 1:1 stoichiometry, it is difficult to attribute any function to TatB alone. TatA, on the other hand, has been studied on its own and has been shown to have interesting properties by itself (18, 19, 22, 38, 46, 60). We interpret the detrimental effects of TatA TMH shortening and lengthening differently. We note that while the Ad2 deletion mutant has considerably better activity than any addition mutants (Figs. 5*C* and 6*B*), which suggests that the increased hydrophobic mismatch confers some advantage, it still does not perform as well as the wt. This decline in Tat activity when the TatA TMH is shortened could be attributed in part or in full to a loss of PMF driving force because of induced membrane leakage to protons.

The TatA TMH addition mutants also display poor Tat activity, although we believe there is a different mechanism at work here. We favor the hypothesis that Tat protein transport occurs through transient toroidal pores that form in the membrane as a result of bilayer breakdown in response to localized membrane thinning (6, 21, 25, 61). In this model, the hydrophobic mismatch set up by the Tat subunits confers a natural advantage toward membrane thinning, and this would be intensified by the binding of more TatAs with their short TMHs to the active machinery as the latter assembles on demand (15). Further, extrapolating the effect of the PMF on thinning of the thylakoid membrane (62–64) to the *E. coli* plasma membrane as well provides an immediate mechanism for coupling the PMF to Tat protein transport. Alterations in membrane thickness as a critical determinant of membrane protein function and/or assembly have recently been noted by others (65–70). In this context, one might expect that hydrophobic mismatch in the Tat translocation machinery would play a key role in Tat transport. Accordingly, the tuning of the TatA and TatB TMHs to 15 amino acids might be seen as an evolutionary compromise of selecting a hydrophobic mismatch that is not so severe as to cause detrimental ion leakage but still sufficient to allow the membrane to thin enough under physiological conditions to the point of toroidal pore formation.

Experimental procedures

Strain and plasmid construction

E. coli strain DADE-A (MC4100, *ΔtatABC*, *ΔtatE*, and arabinose resistance) was used in both *in vivo* and *in vitro* experiments in this study (71). For TatA and TatB variants in pTat101 (pTH19Kr derivative, a low copy plasmid constitutively expressing TatABC) (43), the indicated deletion and addition mutations were introduced by QuikChange site-directed mutagenesis (Q5 Site-Directed Mutagenesis Kit; NEB). For TatA variants in pBAD33 (a vector with arabinose-inducible araBAD operon) (72), the appropriate *tatA* mutant alleles were amplified from the corresponding constructs in pTat101, which were then assembled into pBAD33 using the Gibson assembly approach (73). The 6× His tag was inserted into the indicated TatA constructs in pTat101 using the primers TatAhis_F (5′-CAC CAC CAC TAA CAC GTG TTT GAT ATC G-3′) and TatAhis_R (5′-ATG ATG ATG CAC CTG CTC TTT ATC GTG-3′). For TatA constructs in pBAD33, the 6× His tag was added using the primers pBAD33TatAhis_F (5′-TCA CCA CCA CTA ATG GCT GTT

TTG GCG G-3′) and pBAD33TatAhis_R (5′-TGA TGA TGA CCC ACC TGC TCT TTA TCG TG-3′). For *in vivo* transport experiments, construct of pQE80l (SufI-FLAG) was produced as described (74). For pulse-chase experiments, constructs pNR14 and pNR42 were as described previously (75, 76). All constructs were confirmed by Sanger sequencing. More detailed information about the plasmids used in this study can be found in Table S1.

Sequence alignments and sequence logo plots

About 122 TatA sequences and 60 TatB sequences were downloaded from GenBank (National Center for Biotechnology Information). Multiple sequence alignment for TatA and TatB, respectively, was performed using MUSCLE (77). Sequence logos were subsequently generated using RStudio (version 1.3.1073) with the ggseqlogo package (78).

Liquid SDS-growth assay

Overnight cultures grown at 37 °C were normalized to an absorbance of 0.1 at 600 nm before adding to the LB medium containing 0%, 1%, 2%, 5%, or 10% SDS, respectively, to a final absorbance of 0.002. After 5 h of shaking at 37 °C, the absorbance of the cell suspension at 600 nm was measured. Survival rates of the cells in the LB with corresponding SDS concentrations were calculated by taking the ratio of the absorbance of cells grown in LB with indicated SDS concentration to cells grown in the LB without SDS.

In vivo *transport assay*

pTat101 variants were cotransformed with pQE80l (SufI-FLAG) into the DADE-A strain. Cells were first grown overnight at 37 °C and then diluted to an absorbance of 0.06 at 600 nm and cultured in 5 ml of fresh LB medium at 37 °C with shaking for 3 h. SufI-FLAG was induced by the addition of 1 mM IPTG. Following 2.5 h of growth at 37 °C, cells were harvested and subjected to fractionation. For TatA deletion mutants in pBAD33 variants, plasmids containing indicated mutated *tatA* alleles in pBAD33 were cotransformed with pQE80l (SufI-FLAG) and pTat101 or the corresponding pTat101 variants. Overnight cultures were diluted and subcultured in 5 ml of fresh LB medium containing arabinose concentration ranging from 0% to 0.2%. At an absorbance of ∼0.6 at 600 nm, cells were induced with 1 mM IPTG. Following 2.5 h of growth at 37 °C, cells were harvested and subjected to fractionation.

Cell fractionation

After *in vivo* transport, cells were harvested. The volume of cells in each mutant was normalized based on cell densities such that each sample contained 3 ml of cells with absorbance of 1.5 at 600 nm. Cells were centrifuged at 16,000 x *g* at room temperature. Cells were then cooled on ice and fractionated using the EDTA/lysozyme/cold osmotic shock method (79) by applying 80 μl of 1× TES buffer (200 mM Tris–HCl, pH 8.0, 0.5 mM EDTA, and 0.5 M sucrose), 3.2 μl of 10 mg/ml freshly prepared lysozyme solution, and 288 μl of 0.5× TES buffer (1× TES buffer diluted twice in water [v/v]), in order. Samples were then incubated at 4 °C for 30 min before centrifugation at 5000 x *g* for 5 min at 4 °C. Supernatants were kept as the periplasmic fractions by adding equal volume of 2× SDS sample buffer and were subjected to SDS-PAGE/Western blot analyses. For membrane extraction, pellets were then resuspended in 0.5× TES buffer containing 2 mM PMSF, 2 mM $MgCl_2$, and 10 μg/ml DNase I, followed by four cycles of freezing and thawing in liquid nitrogen and centrifugation at 2000 x *g* at 4 °C. For carbonate washed samples, cells were washed in 10 mM Na_2CO_3 for 1 h followed by ultracentrifugation at 120,000 x *g* for 45 min at 4 °C. Pellets were kept as the membrane fraction, which were then subjected to SDS-PAGE/Western blot analyses.

SDS-PAGE and Western blot

Proteins were separated by SDS-PAGE followed by Western blot using anti-TatA, anti-TatB, anti-His tag (GenScript), or anti-FLAG (GenScript) antibodies, depending on the protein samples. 6× His, TatA, and TatB were detected by horseradish peroxide–conjugated anti-rabbit antibody, and SufI-FLAG was detected using horseradish peroxide–conjugated antimouse antibody. Proteins were then visualized using the ProSignal Pico ECL Western Blotting detection kit (Genesee Scientific).

Pulse-chase experiment and autoradiography

Experimental procedures were derived (76). Overnight cultures carrying Tat variants in pTat101, pNR42, and pNR14 were grown in LB media at 30 °C. About 100 μl of the overnight culture was then added in 3 ml of fresh LB media for subculture at 30 °C. After 1.5 h, cells were harvested and normalized such that each sample contained an equivalent of 0.5 ml cells with absorbance of 0.2 at 600 nm. Cells were then washed with 1× M9 medium (M9 salt, 0.1 mM $CaCl_2$, 0.002% thiamine, 2 mM $MgSO_4$, and a 0.01% 18-amino acid mix free of methionine and cysteine) to remove excess LB medium and resuspended in 2.5 ml M9 medium. Cells were grown for another hour at 30 °C. Subsequently, cells were grown at 42 °C for 15 min to induce transcription of T7 polymerase from pNR42. About 400 μg/ml rifampicin were added to inhibit the *E. coli* endogenous RNA polymerase, followed by another 10 min of growth at 42 °C. Cells were incubated for another 20 min at 30 °C. Subsequently, cells were transferred to 37 °C until the completion of the experiment. 0.025 mCi of [^{35}S] methionine (PerkinElmer, Inc; NEG772002MC) was added to 2.5 ml of culture to initiate the pulse process. After 5 min of pulse, cells were chased by adding 750 μg/ml unlabeled cold methionine. A 300 μl sample was taken at each time point, followed by immediate freezing in liquid nitrogen. Samples were then thawed on ice, centrifuged, resuspended with 50 μl 2× SDS sample buffer, and then subjected to SDS-PAGE and autoradiography. Quantification of the protein bands was carried out using ImageJ software (80).

Statistical analysis

Data from the pulse-chase experiments were subjected to statistical analysis. An exponential plateau model, $Y = (Y_m - Y_0) \times e^{-kx}$, which is derived from the first-order reaction model,

was used to fit the data using GraphPad Prism, version 8.2.1, for Windows (GraphPad Software, Inc). The ordinate value corresponds to the mature-to-total ratio for each sample, and the abscissa represents time in the pulse-chase experiment. Y_m was defined as the maximum value of the mature to total (*i.e.*, mature to the sum of the mature and precursor), the initial velocity V_0 was obtained from the model ($V_0 = Y_m \times k$), with the units of the reciprocal minutes.

Statistical analysis of single-pass membrane proteins

A total number of 9232 single-pass membrane protein sequences from four categories (495 from *E. coli*, 5468 from proteobacteria, 2146 from chloroplasts, and 1397 from mitochondria) were downloaded from Swiss-Prot database (81) by selecting single-pass proteins, followed by selecting the corresponding categories. The transmembrane domains of the proteins were then identified by using the TMHMM Server, version 2.0, DTU Health Tech (82). The output of the expected number of amino acids in the TMH per protein was subsequently collected. The amino acid numbers predicted in the TMHs were rounded to the closest integer, and their relative frequency (*i.e.*, ratio of occurrence to the total number of proteins in the indicated category) was plotted against the TMH length for each category using GraphPad Prism, version 8.2.1.

Proton leakage measurement

Plasmids carrying wt or indicated TatA variants with the 6× His tag in pBAD33 were cotransformed with or without TatA in pTat101 separately into DADE-A. IMV preparation was performed as described (83). Acridine orange fluorescence–quenching assays were performed on a Fluorolog-3 spectrofluorometer (HORIBA Scientific; model no.: FL3-22). About 50 μl IMVs (final absorbance at 280 nm = 0.375) were added to a 2 ml reaction master mix containing 1× TE buffer (25 mM MOPS, 25 mM MES, 5 mM $MgCl_2$, 50 mM KCl, 200 mM sucrose, and 57 μg/ml bovine serum albumin, pH = 7.0), 2.9 mM phosphocreatine, 0.29 mg/ml creatine kinase, and 2 μM acridine orange. The reaction mix was kept on ice before the measurement. Before the measurement, the mixture was first incubated in a 3 ml cuvette at 37 °C for 5 min with slow stirring for temperature equilibration. Acridine orange fluorescence was recorded at $\lambda_{excitation}$ = 494 nm (slit = 1 nm) and $\lambda_{emission}$= 540 nm (slit = 5 nm) every 1/10 s. About 20 μl of 400 mM ATP (4 mM final concentration) was added into the cuvette at 60 s, and 4 μl of 5 mM carbonyl cyanide *m*-chlorophenylhydrazone) (10 μM final concentration) was added to the cuvette to dissipate the proton gradient at 200 s.

Data availability

All data are contained within the article.

Supporting information—This article contains supporting information (Supplemental Figures S1-S3, and Table S1).

Acknowledgments—We thank Tracy Palmer and Jon Cherry for their generous gifts of materials as well as for their comments and discussions on this project. We also thank Ben Berks and Thomas Brüser for their many insightful comments on this work.

Author contributions—B. H. and S. M. T. conceptualization; B. H. and W. Z. methodology; W. Z. software; B. H. and W. Z. validation; B. H. and W. Z. formal analysis; B. H. and W. Z. investigation; B. H. and W. Z. data curation; B. H. writing–original draft; B. H., W. Z., and S. M. T. writing–review and editing; B. H. and W. Z. visualization; S. M. T. supervision; S. M. T. project administration; S. M. T. funding acquisition.

Funding and additional information—The work was supported by the Division of Chemical Sciences, Geosciences, and Biosciences, Office of Basic Energy Sciences of the U.S. Department of Energy through Grant DE-SC0020304 to S.M.T.

Conflict of interest—The authors declare that they have no conflicts of interest with the contents of this article.

Abbreviations—The abbreviations used are: ACa, TatA C-terminus addition; Ad, TatA deletion; ANa, TatA N-terminus addition; APH, amphipathic helix; A8Qa, TatA 8th Glutamine addition; BCa, TatB C-terminus addition; Bd, TatB deletion; B8Ea, TatB 8th Glutamate addition; BNa, TatB N-terminus addition; IMV, inverted membrane vesicle; PMF, proton motive force; Tat, twin-arginine translocation; TES, Tris, EDTA, sucrose buffer; TMH, transmembrane alpha helix.

References

1. Clark, S. A., and Theg, S. M. (1997) A folded protein can be transported across the chloroplast envelope and thylakoid membranes. *Mol. Biol. Cell.* **8**, 923–934
2. Ize, B., Stanley, N. R., Buchanan, G., and Palmer, T. (2003) Role of the Escherichia coli Tat pathway in outer membrane integrity. *Mol. Microbiol.* **48**, 1183–1193
3. Palmer, T., Sargent, F., and Berks, B. C. (2005) Export of complex cofactor-containing proteins by the bacterial Tat pathway. *Trends Microbiol.* **13**, 175–180
4. New, C. P., Ma, Q., and Dabney-Smith, C. (2018) Routing of thylakoid lumen proteins by the chloroplast twin arginine transport pathway. *Photosynth. Res.* **138**, 289–301
5. Braun, N. A., Davis, A. W., and Theg, S. M. (2007) The chloroplast Tat pathway utilizes the transmembrane electric potential as an energy source. *Biophys. J.* **93**, 1993–1998
6. Asher, A. H., and Theg, S. M. (2021) Electrochromic shift supports the membrane destabilization model of Tat-mediated transport and shows ion leakage during Sec transport. *Proc. Natl. Acad. Sci. U. S. A.* https://doi.org/10.1073/pnas.2018122118
7. Teter, S. A., and Theg, S. M. (1998) Energy-transducing thylakoid membranes remain highly impermeable to ions during protein translocation. *Proc. Natl. Acad. Sci. U. S. A.* **95**, 1590–1594
8. Mori, H., and Cline, K. (2002) A twin arginine signal peptide and the pH gradient trigger reversible assembly of the thylakoid ΔpH/Tat translocase. *J. Cell Biol.* **157**, 205–210
9. Gérard, F., and Cline, K. (2007) The thylakoid proton gradient promotes an advanced stage of signal peptide binding deep within the Tat pathway receptor complex. *J. Biol. Chem.* **282**, 5263–5272
10. Johann, H., Kristoffer, M., Jon, C., Grant, B., J S, P., and Tracy, P. (2017) Substrate-triggered position switching of TatA and TatB during Tat transport in Escherichia coli. *Open Biol.* **7**, 170091
11. Taubert, J., Hou, B., Risselada, H. J., Mehner, D., Lünsdorf, H., Grubmüller, H., *et al.* (2015) TatBC-independent TatA/Tat substrate interactions contribute to transport efficiency. *PLoS One* **10**, e0119761

12. Leake, M. C., Greene, N. P., Godun, R. M., Granjon, T., Buchanan, G., Chen, S., *et al.* (2008) Variable stoichiometry of the TatA component of the twin-arginine protein transport system observed by *in vivo* single-molecule imaging. *Proc. Natl. Acad. Sci. U. S. A.* **105**, 15376–15381
13. Hu, Y., Zhao, E., Li, H., Xia, B., and Jin, C. (2010) Solution NMR structure of the TatA component of the twin-arginine protein transport system from gram-positive bacterium bacillus subtilis. *J. Am. Chem. Soc.* **132**, 15942–15944
14. Pettersson, P., Ye, W., Jakob, M., Tannert, F., Klösgen, R. B., and Mäler, L. (2018) Structure and dynamics of plant TatA in micelles and lipid bilayers studied by solution NMR. *FEBS J.* **285**, 1886–1906
15. Rollauer, S. E., Tarry, M. J., Graham, J. E., Jääskeläinen, M., Jäger, F., Johnson, S., *et al.* (2012) Structure of the TatC core of the twin-arginine protein transport system. *Nature* **492**, 210–214
16. Zhang, Y., Wang, L., Hu, Y., and Jin, C. (2014) Solution structure of the TatB component of the twin-arginine translocation system. *Biochim. Biophys. Acta* **1838**, 1881–1888
17. Frain, K. M., Robinson, C., and van Dijl, J. M. (2019) Transport of folded proteins by the Tat system. *Protein J.* https://doi.org/10.1007/s10930-019-09859-y
18. Gohlke, U., Pullan, L., McDevitt, C. A., Porcelli, I., de Leeuw, E., Palmer, T., *et al.* (2005) The TatA component of the twin-arginine protein transport system forms channel complexes of variable diameter. *Proc. Natl. Acad. Sci. U. S. A.* **102**, 10482–10486
19. Hauer, R. S., Freudl, R., Dittmar, J., Jakob, M., and Klösgen, R. B. (2017) How to achieve Tat transport with alien TatA. *Sci. Rep.* **7**, 1–13
20. Hauer, R. S., Schlesier, R., Heilmann, K., Dittmar, J., Jakob, M., and Klösgen, R. B. (2013) Enough is enough: TatA demand during Tat-dependent protein transport. *Biochim. Biophys. Acta* **1833**, 957–965
21. Brüser, T., and Sanders, C. (2003) An alternative model of the twin arginine translocation system. *Microbiol. Res.* **158**, 7–17
22. Hou, B., Heidrich, E. S., Mehner-Breitfeld, D., and Brüser, T. (2018) The TatA component of the twin-arginine translocation system locally weakens the cytoplasmic membrane of Escherichia coli upon protein substrate binding. *J. Biol. Chem.* **293**, 7592–7605
23. Van den Berg, B., Clemons, W. M., Collinson, I., Modis, Y., Hartmann, E., Harrison, S. C., *et al.* (2004) X-ray structure of a protein-conducting channel. *Nature* **427**, 36–44
24. Tsirigotaki, A., De Geyter, J., Šoštarić, N., Economou, A., and Karamanou, S. (2017) Protein export through the bacterial Sec pathway. *Nat. Rev. Microbiol.* **15**, 21–36
25. Chen, F.-Y., Lee, M.-T., and Huang, H. W. (2003) Evidence for membrane thinning effect as the mechanism for peptide-induced pore formation. *Biophys. J.* **84**, 3751–3758
26. Huan, Y., Kong, Q., Mou, H., and Yi, H. (2020) Antimicrobial peptides: classification, design, application and research progress in multiple fields. *Front. Microbiol.* **11**, 582779 [online]
27. Lee, M.-T., Sun, T.-L., Hung, W.-C., and Huang, H. W. (2013) Process of inducing pores in membranes by melittin. *Proc. Natl. Acad. Sci. U. S. A.* **110**, 14243–14248
28. Brown, K. L., and Hancock, R. E. (2006) Cationic host defense (antimicrobial) peptides. *Curr. Opin. Immunol.* **18**, 24–30
29. Gurtovenko, A. A., and Anwar, J. (2007) Modulating the structure and properties of cell membranes: the molecular mechanism of action of dimethyl sulfoxide. *J. Phys. Chem. B.* **111**, 10453–10460
30. Sengupta, D., Leontiadou, H., Mark, A. E., and Marrink, S.-J. (2008) Toroidal pores formed by antimicrobial peptides show significant disorder. *Biochim. Biophys. Acta* **1778**, 2308–2317
31. Mitra, K., Ubarretxena-Belandia, I., Taguchi, T., Warren, G., and Engelman, D. M. (2004) Modulation of the bilayer thickness of exocytic pathway membranes by membrane proteins rather than cholesterol. *Proc. Natl. Acad. Sci. U. S. A.* **101**, 4083–4088
32. Brandizzi, F., Frangne, N., Marc-Martin, S., Hawes, C., Neuhaus, J.-M., and Paris, N. (2002) The destination for single-pass membrane proteins is influenced markedly by the length of the hydrophobic domain. *Plant Cell* **14**, 1077–1092
33. Milovanovic, D., Honigmann, A., Koike, S., Göttfert, F., Pähler, G., Junius, M., *et al.* (2015) Hydrophobic mismatch sorts SNARE proteins into distinct membrane domains. *Nat. Commun.* **6**, 5984
34. Parton, D. L., Klingelhoefer, J. W., and Sansom, M. S. P. (2011) Aggregation of model membrane proteins, modulated by hydrophobic mismatch, membrane curvature, and protein class. *Biophys. J.* **101**, 691–699
35. Killian, J. A. (1998) Hydrophobic mismatch between proteins and lipids in membranes. *Biochim. Biophys. Acta* **1376**, 401–416
36. Dabney-Smith, C., Mori, H., and Cline, K. (2006) Oligomers of Tha4 organize at the thylakoid Tat translocase during protein transport. *J. Biol. Chem.* **281**, 5476–5483
37. Palmer, T., and Berks, B. C. (2012) The twin-arginine translocation (Tat) protein export pathway. *Nat. Rev. Microbiol.* **10**, 483–496
38. Zhang, Y., Hu, Y., Li, H., and Jin, C. (2014) Structural basis for TatA oligomerization: an NMR study of Escherichia coli TatA dimeric structure. *PLoS One* **9**, e103157
39. Barrett, C. M. L., Mathers, J. E., and Robinson, C. (2003) Identification of key regions within the Escherichia coli TatAB subunits. *FEBS Lett.* **537**, 42–46
40. Perkins, G., Renken, C., Martone, M. E., Young, S. J., Ellisman, M., and Frey, T. (1997) Electron Tomography of neuronal mitochondria: three-dimensional structure and organization of cristae and membrane contacts. *J. Struct. Biol.* **119**, 260–272
41. Pribil, M., Labs, M., and Leister, D. (2014) Structure and dynamics of thylakoids in land plants. *J. Exp. Bot.* **65**, 1955–1972
42. Saidijam, M., Azizpour, S., and Patching, S. G. (2018) Comprehensive analysis of the numbers, lengths and amino acid compositions of transmembrane helices in prokaryotic, eukaryotic and viral integral membrane proteins of high-resolution structure. *J. Biomol. Struct. Dyn.* **36**, 443–464
43. Kneuper, H., Maldonado, B., Jäger, F., Krehenbrink, M., Buchanan, G., Keller, R., *et al.* (2012) Molecular dissection of TatC defines critical regions essential for protein transport and a TatB–TatC contact site. *Mol. Microbiol.* **85**, 945–961
44. Kim, H., Botelho, S. C., Park, K., and Kim, H. (2015) Use of carbonate extraction in analyzing moderately hydrophobic transmembrane proteins in the mitochondrial inner membrane. *Protein Sci.* **24**, 2063–2069
45. Behrendt, J., and Brüser, T. (2014) The TatBC complex of the Tat protein translocase in Escherichia coli and its transition to the substrate-bound TatABC complex. *Biochemistry* **53**, 2344–2354
46. Alcock, F., Baker, M. A. B., Greene, N. P., Palmer, T., Wallace, M. I., and Berks, B. C. (2013) Live cell imaging shows reversible assembly of the TatA component of the twin-arginine protein transport system. *Proc. Natl. Acad. Sci. U. S. A.* **110**, E3650–E3659
47. Rose, P., Fröbel, J., Graumann, P. L., and Müller, M. (2013) Substrate-dependent assembly of the Tat translocase as observed in live Escherichia coli cells. *PLoS One* **8**, e69488
48. Celedon, J. M., and Cline, K. (2012) Stoichiometry for binding and transport by the twin arginine translocation system. *J. Cell Biol.* **197**, 523–534
49. Rodriguez, F., Rouse, S. L., Tait, C. E., Harmer, J., Riso, A. D., Timmel, C. R., *et al.* (2013) Structural model for the protein-translocating element of the twin-arginine transport system. *Proc. Natl. Acad. Sci. U. S. A.* **110**, E1092–E1101
50. Alcock, F., Stansfeld, P. J., Basit, H., Habersetzer, J., Baker, M. A., Palmer, T., *et al.* (2016) Assembling the Tat protein translocase. *eLife* **5**, e20718
51. [preprint] Mól, A. R., Castro, M. S., and Fontes, W. (2018) NetWheels: a web application to create high quality peptide helical wheel and net projections. *bioRxiv*. https://doi.org/10.1101/416347
52. Greene, N. P., Porcelli, I., Buchanan, G., Hicks, M. G., Schermann, S. M., Palmer, T., *et al.* (2007) Cysteine scanning mutagenesis and disulfide mapping studies of the TatA component of the bacterial twin arginine translocase. *J. Biol. Chem.* **282**, 23937–23945
53. de Planque, M. R. R., Bonev, B. B., Demmers, J. A. A., Greathouse, D. V., Koeppe, R. E., Separovic, F., *et al.* (2003) Interfacial anchor properties of tryptophan residues in transmembrane peptides can dominate over hydrophobic matching effects in peptide– lipid interactions. *Biochemistry* **42**, 5341–5348

54. Jaud, S., Fernández-Vidal, M., Nilsson, I., Meindl-Beinker, N. M., Hübner, N. C., Tobias, D. J., *et al.* (2009) Insertion of short transmembrane helices by the Sec61 translocon. *Proc. Natl. Acad. Sci. USA* **106**, 11588–11593
55. Ulmschneider, J. P. (2018) Molecular dynamics simulations are redefining our view of peptides interacting with biological membranes. *Acc. Chem. Res.* **51**, 1106–1116
56. Aldridge, C., Storm, A., Cline, K., and Dabney-Smith, C. (2012) The chloroplast twin arginine transport (Tat) component, Tha4, undergoes conformational changes leading to Tat protein transport. *J. Biol. Chem.* **287**, 34752–34763
57. Dabney-Smith, C., Mori, H., and Cline, K. (2003) Requirement of a Tha4-conserved transmembrane glutamate in thylakoid Tat translocase assembly revealed by biochemical complementation. *J. Biol. Chem.* **278**, 43027–43033
58. Frielingsdorf, S., Jakob, M., and Klösgen, R. B. (2008) A stromal pool of TatA promotes Tat-dependent protein transport across the thylakoid membrane. *J. Biol. Chem.* **283**, 33838–33845
59. Pettersson, P., Patrick, J., Jakob, M., Jacobs, M., Klösgen, R. B., Wennmalm, S., *et al.* (2021) Soluble TatA forms oligomers that interact with membranes: structure and insertion studies of a versatile protein transporter. *Biochim. Biophys. Acta Biomembr.* **1863**, 183529
60. Celler, K., van Wezel, G. P., and Willemse, J. (2013) Single particle tracking of dynamically localizing TatA complexes in Streptomyces coelicolor. *Biochem. Biophys. Res. Commun.* **438**, 38–42
61. Berks, B. C. (2015) The twin-arginine protein translocation pathway. *Annu. Rev. Biochem.* **84**, 843–864
62. Johnson, M. P., Goral, T. K., Duffy, C. D. P., Brain, A. P. R., Mullineaux, C. W., and Ruban, A. V. (2011) Photoprotective energy dissipation involves the reorganization of photosystem II light-harvesting complexes in the grana membranes of spinach chloroplasts. *Plant Cell* **23**, 1468–1479
63. Kirchhoff, H., Hall, C., Wood, M., Herbstová, M., Tsabari, O., Nevo, R., *et al.* (2011) Dynamic control of protein diffusion within the granal thylakoid lumen. *Proc. Natl. Acad. Sci. U. S. A.* **108**, 20248–20253
64. Murakami, S., and Packer, L. (1970) Light-induced changes in the conformation and configuration of the thylakoid membrane of ulva and porphyra chloroplasts *in vivo*. *Plant Physiol.* **45**, 289–299
65. Chen, Y., Capponi, S., Zhu, L., Gellenbeck, P., Freites, J. A., White, S. H., *et al.* (2017) YidC insertase of Escherichia coli: water accessibility and membrane shaping. *Structure* **25**, 1403–1414.e3
66. He, Y., Xu, J., Wu, X., and Li, L. (2020) Structures of a P4-ATPase lipid flippase in lipid bilayers. *Protein Cell* **11**, 458–463
67. Iadanza, M. G., Schiffrin, B., White, P., Watson, M. A., Horne, J. E., Higgins, A. J., *et al.* (2020) Distortion of the bilayer and dynamics of the BAM complex in lipid nanodiscs. *Commun. Biol.* **3**, 1–14
68. Kreutzberger, A. J. B., Ji, M., Aaron, J., Mihaljević, L., and Urban, S. (2019) Rhomboid distorts lipids to break the viscosity-imposed speed limit of membrane diffusion. *Science*. https://doi.org/10.1126/science.aao0076
69. Pleiner, T., Tomaleri, G. P., Januszyk, K., Inglis, A. J., Hazu, M., and Voorhees, R. M. (2020) Structural basis for membrane insertion by the human ER membrane protein complex. *Science* **369**, 433–436
70. Wu, X., Siggel, M., Ovchinnikov, S., Mi, W., Svetlov, V., Nudler, E., *et al.* (2020) Structural basis of ER-associated protein degradation mediated by the Hrd1 ubiquitin ligase complex. *Science* **368**, eaaz2449
71. Wexler, M., Sargent, F., Jack, R. L., Stanley, N. R., Bogsch, E. G., Robinson, C., *et al.* (2000) TatD is a cytoplasmic protein with DNase activity NO requirement for TatD family proteins IN sec-independent protein export. *J. Biol. Chem.* **275**, 16717–16722
72. Guzman, L. M., Belin, D., Carson, M. J., and Beckwith, J. (1995) Tight regulation, modulation, and high-level expression by vectors containing the arabinose PBAD promoter. *J. Bacteriol.* **177**, 4121–4130
73. Gibson, D. G., Young, L., Chuang, R.-Y., Venter, J. C., Hutchison, C. A., and Smith, H. O. (2009) Enzymatic assembly of DNA molecules up to several hundred kilobases. *Nat. Methods* **6**, 343–345
74. Huang, Q., and Palmer, T. (2017) Signal peptide hydrophobicity modulates interaction with the twin-arginine translocase. *mBio* **8**, e00909–e00917
75. Sargent, F., Stanley, N. R., Berks, B. C., and Palmer, T. (1999) Sec-independent protein translocation in Escherichia coli. *J. Biol. Chem.* **274**, 36073–36082
76. Stanley, N. R., Palmer, T., and Berks, B. C. (2000) The twin arginine consensus motif of Tat signal peptides is involved in Sec-independent protein targeting in Escherichia coli. *J. Biol. Chem.* **275**, 11591–11596
77. Edgar, R. C. (2004) Muscle: a multiple sequence alignment method with reduced time and space complexity. *BMC Bioinform.* **5**, 113
78. Wagih, O. (2017) ggseqlogo: a versatile R package for drawing sequence logos. *Bioinformatics* **33**, 3645–3647
79. Petiti, M., Houot, L., and Duché, D. (2017) Cell fractionation. In: Journet, L., Cascales, E., eds., *Methods in Molecular BiologyBacterial Protein Secretion Systems: Methods and Protocols*, Springer, New York, NY: 59–64. https://doi.org/10.1007/978-1-4939-7033-9_3
80. Schneider, C. A., Rasband, W. S., and Eliceiri, K. W. (2012) NIH image to ImageJ: 25 years of image analysis. *Nat. Methods* **9**, 671–675
81. The UniProt Consortium (2021) UniProt: the universal protein knowledgebase in 2021. *Nucl. Acids Res.* **49**, D480–D489
82. Möller, S., Croning, M. D., and Apweiler, R. (2001) Evaluation of methods for the prediction of membrane spanning regions. *Bioinforma. Oxf. Engl.* **17**, 646–653
83. Bageshwar, U. K., and Musser, S. M. (2007) Two electrical potential–dependent steps are required for transport by the Escherichia coli Tat machinery. *J. Cell Biol.* **179**, 87–99